Journal of Applied Polymer Science

Dielectric and Thermal Studies of Segmental Dynamics in Silica/PDMS and Silica/Titania/PDMS Nanocomposites

Iryna Sulym,[1] Panagiotis Klonos,[2] Mykola Borysenko,[1] Polycarpos Pissis,[2] Vladimir M. Gun'ko[1]
[1]Chuiko Institute of Surface Chemistry, 17 General Naumov Street, 03164 Kyiv, Ukraine
[2]Department of Physics, National Technical University of Athens, 15780 Athens, Greece
Correspondence to: I. Sulym (E-mail: sulim1981@mail.ru)

ABSTRACT: Effects of silica and silica/titania nanoparticles on glass transition and segmental dynamics of poly(dimethylsiloxane) (PDMS) were studied for composites of a core–shell type using differential scanning calorimetry, thermally stimulated depolarization current, and dielectric relaxation spectroscopy techniques. Strong interactions between the filler and the polymer suppress crystallinity (T_c, X_c) and affect significantly the evolution of the glass transition in the nanocomposites. The segmental relaxation associated with the glass transition consists of three contributions, arising, in the order of decreasing mobility, from the bulk (unaffected) amorphous polymer fraction (α relaxation), from polymer chains restricted between condensed crystal regions (α_c relaxation), and from the semi-bound polymers in an interfacial layer with strongly reduced mobility due to interactions with surface hydroxyls of silica and silica/titania nanoparticles (α' relaxation). The evolution of surface affected CH_3 groups, as well as the degree of interaction of PDMS molecules with surface hydroxyl groups as a function of treatment temperature, was assessed by Fourier transform infrared spectroscopy, thermogravimetry and differential thermal analysis. The effectiveness of silica/PDMS and silica/titania/PDMS nanocomposites as hydrophobic coatings was investigated by static contact angle measurements. It was shown that the presence of titania nanoparticles and adsorbed PDMS promotes the hydrophobic properties of the PDMS coating after treatment in the 80–650°C range. © 2014 Wiley Periodicals, Inc. J. Appl. Polym. Sci. **2014**, *131*, 41154.

KEYWORDS: composites; crystallization; dielectric properties; differential scanning calorimetry; glass transition

Received 12 March 2014; accepted 12 June 2014
DOI: 10.1002/app.41154

INTRODUCTION

In recent years, polymer nanocomposites have attracted significant interest due to their synergistic and hybrid properties derived from several components. These materials offer unique mechanical,[1] electrical,[2] optical,[2] thermal,[3,4] and bioactive properties, especially suitable for their applications as sensors, nonlinear optical materials, selective membranes, catalysts, and protective coating.[5,6]

Silica–poly(dimethylsiloxane) (PDMS) composite is one of important systems among hybrid materials.[7–9] PDMS is the most important and widely used siloxane polymer.[1–10] It is well known as a high-performance material because of its extremely low glass transition temperature (−125°C) and high thermal stability compared with those of other elastomers. The helix shape of PDMS with six O—Si—O bonds in a cycle[10] restricts the number of segments which can directly interact with a matrix surface to form hydrogen bonds ≡SiO—H···O(Si$(CH_3)_2$—)$_2$ or bonding due to dispersion interactions. However, the PDMS conformation can be changed in the adsorption layer depending on the PDMS content.

It is commonly accepted that the improvement of properties of polymer nanocomposites is linked to modified polymer dynamics in the interfacial layer.[11,12] A variation in the PDMS content in composites can affect many properties of the whole material. Very often the presence of various nanofillers, such as silica, titania, and so forth, leads to a restriction of polymer mobility and thermal transition ability manifested in an increase in glass transition temperature and a decrease in the degree of crystallinity and the crystallization temperature in semi-crystalline polymer matrices.[13]

Effects of silica interlayer distance on the polymer T_g values of nanocomposites made from doubly supported films were previously studied.[14] It was found that interfacial interactions, which yield significant increases in T_g in nanocomposites, may yield much more significant effects on other glassy behavior such as physical ageing. The similar results were obtained by Torkelson et al.[15] It was shown that both real and model nanocomposites demonstrate strong suppressions of physical aging relative to bulk polymer. This suggests that nanocomposites may have important technological applications related to the production of glassy-state polymeric materials with properties that are much less subject to

physical aging than neat polymers. This provides the possibility to conduct studies that will allow understanding how the separation distance between nanofiller interfaces impacts the glass transition and physical aging of the polymer.

Thus, understanding interfacial chemistry is important for ultimate engineering of the mechanical, electrical or chemical properties. Generally, the improved properties of polymer-containing nanocomposites are related to the modification of the structure and dynamics of a polymer phase due to interactions with a filler surface. So, in-depth studies of interfacial interactions between a filler surface and associated polymer chains are warranted. Notice that PDMS is frequently used in different applications including bioengineering and other bioapplications.[16–28] Nanocomposites can be more effective materials than individual polymers for these applications.

In our previous works,[29,30] it has been shown that many properties (such as structural characteristics of the composites, reactions during heating in air and vacuum, interfacial relaxation phenomena, hydrophobicity as a function of treatment temperature, etc.) of PDMS/zirconia/silica strongly differ from those of PDMS/silica. Broadening of the α relaxation of PDMS at the interfaces of disperse oxides suggests both weakening of the PDMS–PDMS interactions and strengthening of the PDMS–oxide interactions.[29] Notice that the interfacial behavior of PDMS depends strongly on the morphology and texture of oxides in the oxide/PDMS composites.[31,32]

Despite numerous investigations of polysiloxane materials (notice that most of them are related to linear poly(R_2-siloxane) such as PDMS),[1,3–6,31] deeper understanding of the behavior of interfacial layers of PDMS adsorbed onto chemically different highly disperse oxides with different textural porosity needs additional investigations.

Therefore, in the present work the effects of silica and silica/titania nanoparticles on glass transition and segmental dynamics of PDMS have been studied. Differential scanning calorimetry (DSC), thermally stimulated depolarization currents (TSDC) and dielectric relaxation spectroscopy (DRS) techniques, covering together a broad frequency range from 10^{-4} to 10^{6} Hz, are used here. Infrared spectroscopy technique is used to obtain information on surface affected groups and the degree of interaction of PDMS molecules with surface hydroxyls. Thermal destruction of PDMS adsorbed on a surface of initial fumed silica and SiO_2/TiO_2 has been also studied using thermogravimetry (TG) and differential thermal analysis. The hydrophilic/hydrophobic properties of the composites are characterized by the values of the contact angle of settled water drops.

EXPERIMENTAL

Materials

Pyrogenic (fumed) silica PS300 (pilot plant of the Chuiko Institute of Surface Chemistry, Kalush, Ukraine, specific surface area $S = 290$ m^2/g) and binary oxide SiO_2/TiO_2 (ST) ($S = 174$ m^2/g) were used as substrates for adsorption modification by PDMS. Silica/titania was synthesized through the interaction of nanosilica PS175 (pilot plant of the Chuiko Institute of Surface Chemistry, $S = 185$ m^2/g) with $TiCl_4$ (Merck) at $T = 200$°C, subsequent treatment with water vapor,[33,34] and calcination at relatively low temperature (400°C) to prevent titania nanoparticle consolidation. The concentration of TiO_2 was 2.7 wt % and according to XRD measurements titanium dioxide is amorphous, because any crystalline phase is not observed.

Liquid PDMS-1000 ("Kremniypolimer," Zaporozhye, Ukraine; molecular weight $W_m \approx 7960$, degree of polymerization $d_p = 105$, kinematic viscosity 1036 mm^2/s at 20°C) was adsorbed onto initial silica and silica/titania to prepare samples containing 40 wt % of the polymer. Before the adsorption, oxide samples were dried at 110°C for 1 h, and then a solution of PDMS (1 wt %.) in hexane was added and the suspension was stirred. The suspension was dried at room temperature for 24 h and then at 80°C for 3 h.

The hydrophobicity of the samples was estimated from the contact angle values of water drops measured using the sessile drop method with an USB digital microscope (Sigeta, China, magnification from 20× to 200×). A drop of distilled water was seated onto a pressed pellet with oxide/PDMS preheated at 80–700°C for 0.5 h and cooled to room temperature. This treatment results in temperature-dependent degradation of the PDMS layer differently affected by silica and silica/titania surfaces. Measurements were carried out in air at room temperature (18°C). The calculations were made according to standard procedures described in the literature.[35]

Fourier Transform Infrared Spectroscopy

Fourier transform infrared spectroscopy (FTIR) spectra of powdered samples (grinded with KBr at the mass ratio 1 : 9) over the 4000–400 cm^{-1} range were recorded in a diffuse reflectance mode using a ThermoNicolet FTIR spectrometer. For quantitative analysis, some IR spectra were normalized using the intensity of the Si—O vibration overtone at 1865 cm^{-1} as an inner standard.

Specific Surface Area

The specific surface area (S) was calculated using adsorption of argon (from an Ar/He mixture) at 77.4 K using a LKhM-72 (Russia) chromatograph and Silochrome-80 as a reference material.

TG

TG analysis of PDMS adsorbed on oxide samples (weight ≈ 200 mg) was carried out in air at a heating rate of 10°C/min in the 20–1000°C range using a Derivatograph Q-1500D (Paulik, Paulik and Erdey, MOM, Budapest) with TG-DTA (differential thermal analysis).

DSC

Thermal properties of the materials were investigated in helium atmosphere in the temperature range from −175°C to 0°C using a TA Q200 series DSC instrument, calibrated with indium (for temperature and enthalpy) and sapphire (for heat capacity). The samples of ~8 mg in mass were closed in standard aluminum pans. Cooling and heating rates were fixed to 10°C/min. Notice that PDMS crystals are melted at room temperature, so a first heating scan for erasing thermal history[36] was not necessary here.

TSDC

TSDC is a special dielectric technique in the temperature domain, characterized by high sensitivity and high resolving

Table I. Characteristics of Silica/PDMS and Silica/Titania/PDMS Nanocomposites

Sample	Treatment temperature (°°C)	S (m^2/g)
PS300/PDMS	80	265
PS300/PDMS	300	256
PS300/PDMS	400	293
PS300/PDMS	450	307
PS300/PDMS	500	294
PS300/PDMS	600	299
ST/PDMS	80	27
ST/PDMS	300	29
ST/PDMS	400	30
ST/PDMS	450	74
ST/PDMS	500	172
ST/PDMS	600	178

power. The latter arises from a low equivalent frequency (10^{-4}–10^{-2} Hz).[37] By this technique, a sample (powder compressed to form a cylindrical pellet of 12 mm in diameter and 1–2 mm in thickness) was inserted between the brass plates of a capacitor, placed in a Novocontrol TSDC sample cell and polarized by an electrostatic field E_p ($\sim 10^4$ V/m) with a home-made voltage source at polarization temperature $T_p = 20$°C for 5 min. With the field still applied, the sample was cooled down to −150°C (cooling rate 10°C/min, under nitrogen flow), sufficiently low to prevent depolarization by thermal energy, then short-circuited and reheated up to 50°C at a constant heating rate $b = 3$°C/min. Temperature control was achieved by means of a Novocontrol Quatro cryosystem. A discharge current was generated during heating and measured as a function of temperature with a sensitive programmable Keithley 617 electrometer.

DRS

For DRS[38] measurements, the samples (the same used in TSDC measurements) were placed between the plates of a capacitor and an alternate voltage was applied in a Novocontrol sample cell. The complex dielectric permittivity, $\varepsilon^* = \varepsilon' - i\varepsilon''$, was recorded isothermally as a function of frequency in the range from 10^{-1} to 10^6 Hz at temperatures from −150 to 60°C (in nitrogen atmosphere) in steps of 2.5, 5 and 10°C (depending on the process to be studied) using a Novocontrol Alpha analyzer. The temperature was controlled to better than ±0.5°C with a Novocontrol Quatro cryosystem.

RESULTS AND DISCUSSION

Temperature Behavior of Bound PDMS

According to chromatographic measurements (Silochrome at $S = 80$ m^2/g as a reference material) the S value decreases by 9% for PS300 and 83% for ST after PDMS adsorption in amount of 40 wt % (Table I). This result can be explained by larger sizes of the ST particles more strongly agglutinated by the same amount of PDMS in comparison with PDMS/nanosilica with a thinner polymer shell of smaller silica nanoparticles. Oxidizing destruction of the PDMS shell during heating of samples in air up to 600°C leads to an increase in the specific surface area (Table I), which is similar to that of individual oxides.

PDMS macromolecules can form a helix structure due to the corresponding rotations of neighboring $Si(CH_3)_2$ groups around the Si—O bonds.[10] Therefore, only a portion of the segments of adsorbed PDMS molecules can interact with a silica or ST surface, for example, by formation of the hydrogen bonds $\equiv M_iO—H\cdots O(Si(CH_3)_2—)_2$ (where M = Si or Ti, $i = 1$ or 2) and due to dispersion interactions. The dimethylsilyl groups non-interacting with the oxide surface can interact with other PDMS molecules. This effect is stronger for ST/PDMS because of a thicker layer of the polymer located on ST nanoparticles larger than PS300 nanoparticles.

FTIR spectroscopy was used to study the thermal behavior of the PDMS shells on the nanooxide cores at different temperatures (Figure 1). The PDMS adsorption can be analyzed due to

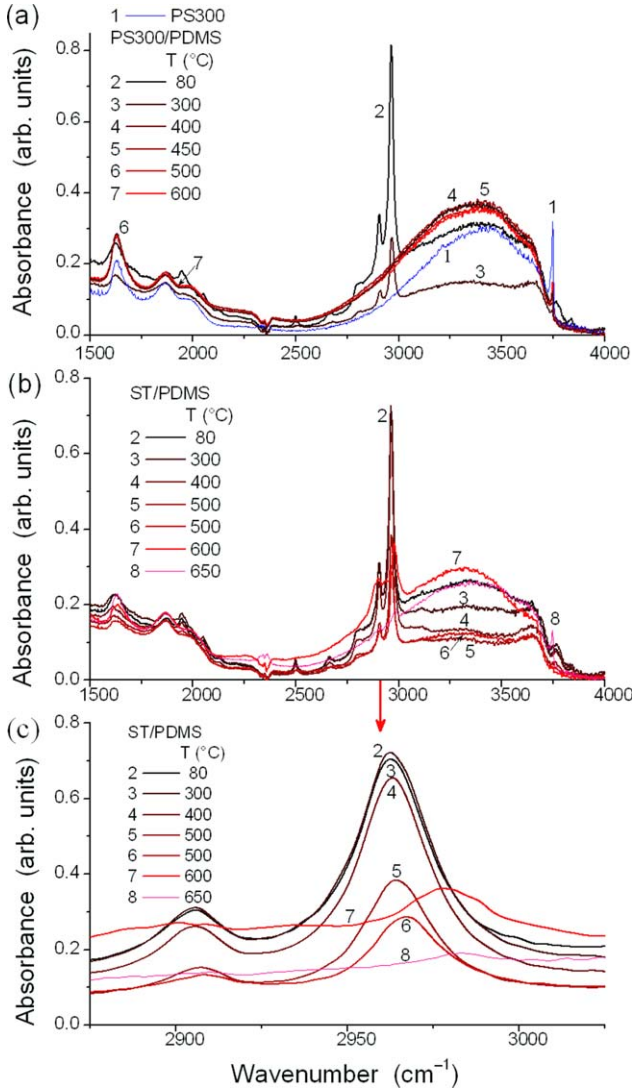

Figure 1. FTIR spectra of PS300 (a, curve 1) and (a) PS300/PDMS and (b and c) ST/PDMS after heating at 80 (2), 300 (3), 400 (4), 450 (5), 500 (6), 600 (7), and 650°C (8) in air for 0.5 h. [Color figure can be viewed in the online issue, which is available at wileyonlinelibrary.com.]

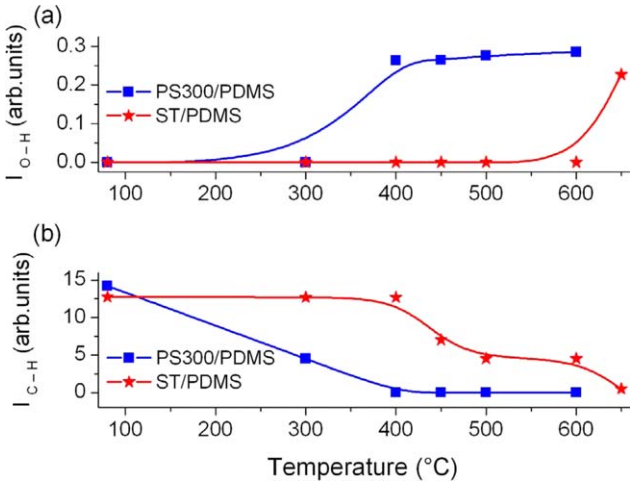

Figure 2. Integral intensity of the bands of (a) the O—H and (b) C—H stretching vibrations of free silanols and CH_3 groups, respectively, as a function of treatment temperature for PS300/PDMS and ST/PDMS at $C_{PDMS} = 40$ wt % in air. [Color figure can be viewed in the online issue, which is available at wileyonlinelibrary.com.]

changes in integral intensity of bands of the O—H ($I_{O—H}$ at 3749 cm^{-1}) and C—H ($I_{C—H}$ at 2969 cm^{-1}) stretching vibrations depending on pretreatment temperature (Figure 2). It was found that the maximal integral intensity of the C—H stretching vibrations (pretreatment at 80°C) decreases by a factor of 3.2 at calcination of PDMS/PS300 at 300°C [Figure 2(b)]. The band of the CH—stretching vibrations of CH_3 groups is absent after sample treatment at 400°C [Figure 1(a), curve 4].

A different picture is observed for PDMS/TS composite demonstrating resistance of dimethylsilyl groups of PDMS up to 400°C. Even after preheating at 600°C, the integral intensity of the C—H stretching vibration band has about 35% of its intensity after preheating at 80°C. Calcination of the sample to 650°C does not lead to complete oxidation of dimethylsilyl groups [Figure 1(b,c) curve 8]. It should be noted that the absorption band of free silanols appears in the FTIR spectra only at 650°C [Figure 1(b)]. There is a certain shift of the ν_{CH} band peak from 2962 cm^{-1} for ST/PDMS preheated at 80°C toward 2978 and 2983 cm^{-1} after heating at 600 and 650°C, respectively [Figure 1(c)]. This is due to a small residual amount of bound PDMS (free of intermolecular interactions) and its fragments (products of depolymerization) reacted with the surface to form Si—O—Si(OH)$(CH_3)_2$ groups. Temperature delay of PDMS decomposition at the ST surface in comparison with PS300/PDMS can be explained by thicker polymer structures at a surface of larger nanoparticles. For instance, removal of PDMS fragments at m/z 207 from bulk PDMS has a maximum at 550°C and strongly decreases at 650°C.[29] This is in agreement with the temperature behavior of PDMS bound to ST.

The influence of hydrophilic nanooxides on thermal destruction of the polymer can be estimated by measuring of the composite hydrophobicity caused by PDMS. The contact angle values [Figure 3] show that both composites demonstrate the hydrophobic properties after preheating at 80°C. Moreover ST/PDMS composites are characterized by larger contact angle values of a water drop than PS300/PDMS. Silica/PDMS composite becomes hydrophilic after heating at 450°C, while ST/PDMS demonstrates the thermal stability of the PDMS coating up to 650°C [Figure 3]. These results are in agreement with FTIR spectroscopy data [Figures 1 and 2] and previous investigations.[29] Thus, the presence of TiO_2 nanoparticles in ST can be considered as a promoter of the hydrophobic properties of the polymeric coating in ST/PDMS. However, this is rather effect of the changes in the particulate morphology and agglutination of PDMS and ST particles into the composite with much lower porosity and surface area than PS300/PDMS.

In air, the thermal decomposition of PDMS adsorbed on the surfaces of PS300 and ST is accompanied by exothermal effects [Figure 4]. The exo-effects at $T_{max} = 340–590$°C corresponded to oxidation of dimethylsilyl groups and removal of volatile cyclic siloxanes.[29] The TG/DTG graphs for PS300/PDMS and ST/PDMS samples exhibit two well-defined regions of the weight loss at 300–600°C coinciding with the temperature range of exothermal effects [Figure 4]. At the same polymer content

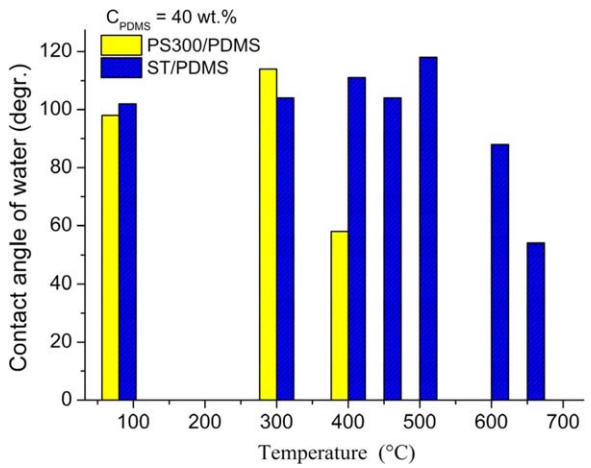

Figure 3. Dependence of the contact angle of water drops located at a surface of pre-heated and pressed nanocomposites on the calcination temperature. [Color figure can be viewed in the online issue, which is available at wileyonlinelibrary.com.]

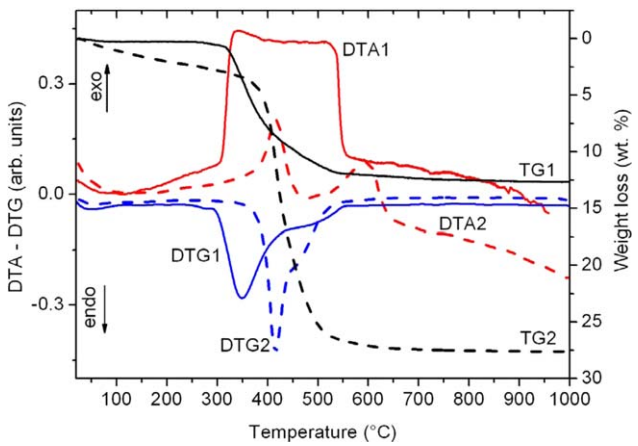

Figure 4. Thermogravimetric (TG), DTA–DTG data for (1) PS300/PDMS and (2) ST/PDMS samples at $C_{PDMS} = 40$ wt %. [Color figure can be viewed in the online issue, which is available at wileyonlinelibrary.com.]

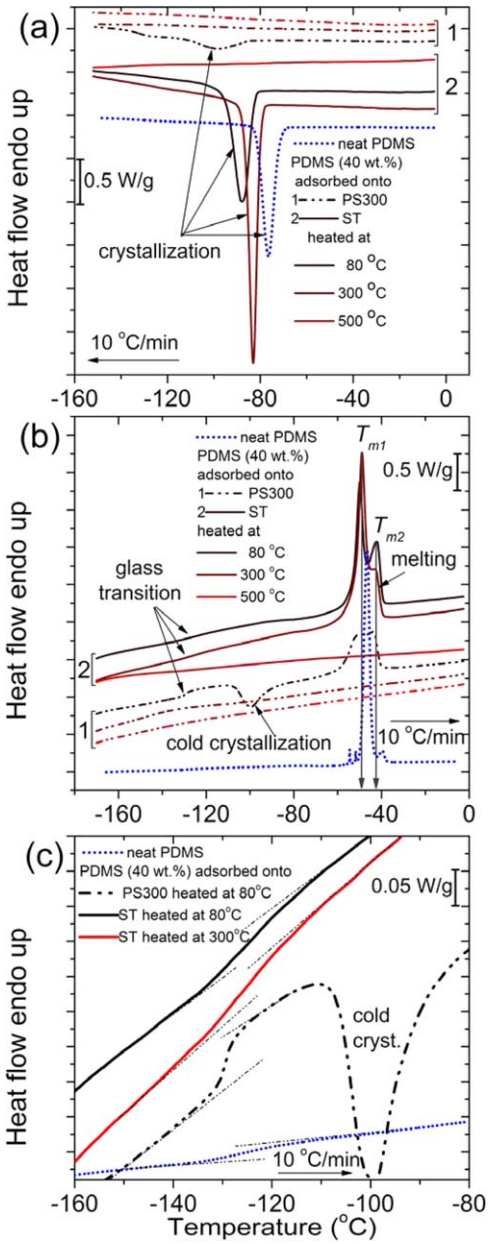

Figure 5. DSC thermograms for initial PDMS, PS300/PDMS and ST/PDMS samples during cooling (a) and subsequent heating (b). The glass transition temperature region during heating is shown in more detail in (c). [Color figure can be viewed in the online issue, which is available at wileyonlinelibrary.com.]

(40 wt %), the values of the weight loss for PS300/PDMS and ST/PDMS composites are 12.5 and 27.5%, respectively, in this temperature range. Previously,[29] it was shown that practically complete oxidation of dimethylsilyl groups occurred at these temperatures in the case of silica/PDMS. The presence of titanium dioxide on silica surface promotes depolymerization of adsorbed PDMS and increasing weight loss. Therefore, one can assume that enhanced stability of the ST coating can be due to effects: (i) thicker PDMS layer on ST than on PS300 nanoparticles; (ii) stronger interactions of the PDMS depolymerization products with the ST surface than with the PS300 surface.

DSC Measurements

DSC measurement results for neat PDMS and nanocomposites are shown for both cooling [Figure 5(a)] and heating [Figure 5(b)] scans. On the basis of these thermograms, the following changes in the thermal transitions of the polymer in the nanocomposites can be analyzed comparing to the neat polymer, as well as effects of the treatment temperature on these transitions. Next to crystallization and melting, we focus here mostly on the glass transition [Figure 5(c)] to analyze the corresponding DSC data in terms of glass transition temperature T_g and heat capacity jump ΔC_p at T_g, which is related to a fraction of polymer participating in the glass transition. All the respective recorded and calculated values of interest are shown in Table II.

Upon cooling scans [Figure 5(a)] a single exothermic peak is observed around −99 to −78°C (T_c), representing the crystallization event, and an endothermic step in the baseline around −129 to −124°C, representing the glass transition of PDMS.[12] The results show that the crystallization temperature decreases significantly in the nanocomposites, from −78°C for neat PDMS to −99 and −88°C for PS300/PDMS and ST/PDMS, respectively.

During heating the glass transition is recorded for all samples and the characteristic temperature T_g is determined as the midpoint of the heat capacity step at glass transition [Figure 5(c), Table II]. For both oxides, T_g decreases by 3–5°C in the nanocomposites, as compared to neat PDMS, and this decrease is stronger for silica due to a thinner PDMS layer. At higher temperatures, −110 to −80°C, cold crystallization effects are observed. The endothermic melting peaks of PDMS crystals are between −60 and −40°C [Figure 5(b)]. The position and the shape of the melting peak(s) depend on the type of the nanocomposite, oxide content and thermal history. The melting temperature (T_{m1}) decreases slightly for PS300/PDMS (−49°C) and ST/PDMS (−50°C) as compared to neat PDMS (−48°C), and the melting peak broadens toward lower temperatures. The secondary weaker melting peak precedes the main one by 5−8°C. The results may be discussed in terms of size and quality of crystals and of primary/secondary crystals affected by both interactions with the oxide surface and certain confined space effects for macromolecules located between adjacent oxide nanoparticles.[11,12,29,39]

Using the crystallization, cold crystallization and melting enthalpies, ΔH_c, ΔH_{cc} and ΔH_m, respectively, recorded by DSC (Table II) and, for comparison, normalized to the same polymer fraction X_{PDMS} for each sample, the degrees of crystallinity $X_{c,\mathrm{cryst}}$ and $X_{c,\mathrm{melt}}$ were calculated, according to eqs. (1) and (2) given below, as it was carried out previously.[11,12] $\Delta H_{100\%}$ in these equations is the enthalpy of PDMS fusion, taken as 37.43 J/g.[39] The heat capacity change recorded by DSC, $\Delta C_{p,\mathrm{DSC}}$, was normalized to the same amorphous polymer fraction according to eq. (3).[11, 12] The results of calculations are presented in Table II.

$$X_{c,\mathrm{cryst}} = \Delta H_c / (X_{\mathrm{PDMS}} \cdot \Delta H_{100\%}) \quad (1)$$

$$X_{c,\mathrm{melt}} = (\Delta H_m - \Delta H_{cc}) / (X_{\mathrm{PDMS}} \cdot \Delta H_{100\%}) \quad (2)$$

$$\Delta C_{p,\mathrm{norm}} = \Delta C_{p,\mathrm{DSC}} / (X_{\mathrm{PDMS}} (1 - X_c)) \quad (3)$$

A main result shown in Table II is that the heat capacity jump at T_g normalized to the same fraction of amorphous polymer,

Table II. Comparison of the Effects of Heating Temperature on the Thermal Characteristics of PDMS ($C = 40$ wt %) Adsorbed onto Initial Silica and Silica/Titania Oxides

	T_c (°C)	ΔH_c (J/g) (±0.5)	$X_{c,cryst}$ (±5 %)	T_g (°C) (±0.5)	$\Delta C_{p,n}$ (J/g·°C) (±0.02)	ΔH_{cc} (J/g) (±0.5)	T_{m1} (°C)	T_{m2}(°C)	ΔH_m (J/g) (±0.5)	$X_{c,melt}$ (±5 %)	$T_{g,diel}$ (°C) (±0.2)
PDMS initial	−78	30	0.80	−124	0.81	30	−48	–	30	–	−124/−129
PS300/PDMS (80°C)	−99	3	0.20	−129	0.25	5	−49	−44	9	0.27	−128
PS300/PDMS (300°C)	–	0	0.00	–	0.00	0	–	–	0	0.00	−130
PS300/PDMS (500°C)	–	0	0.00	–	0.00	0	–	–	0	0.00	–
ST/PDMS (80°C)	−88	10	0.67	−124	0.23	0	−50	−42	12	0.78	−127
ST/PDMS (300°C)	−83	10	0.67	−126	0.15	0	−49	−43	12	0.80	−129
ST/PDMS (500°C)	–	0	0.00	–	0.00	0	–	–	0	0.00	–

Notes: DSC values as recorded from (i) cooling scan: crystallization temperature T_c, crystallization enthalpy ΔH_c and degree of crystallinity as calculated from the crystallization peak $X_{c,cryst}$, (ii) heating scan: temperature and normalized heat capacity change of glass transition T_g and $\Delta C_{p,n}$, respectively, cold crystallization enthalpy ΔH_{cc}, melting peak temperatures T_{m1} and T_{m2}, melting enthalpy ΔH_m, and degree of crystallinity calculated from the melting peak $X_{c,melt}$. DRS value of dielectric glass transition $T_{g,diel}$ for the samples in which α/α_c relaxation mechanism was recorded. For the initial PDMS both α and α_c relaxations where recorded.

$\Delta C_{p,n}$, decreases significantly in the nanocomposites as compared to the neat PDMS. This result suggests that a significant fraction of an amorphous part of the polymer matrix does not contribute to the glass transition. In a simple model, this polymer fraction may be considered as immobilized or interfacial polymer at polymer-filler interfaces relatively strongly interacting with the oxide surface. The interfacial polymer or, at least, a part of it is supposed not to contribute the glass transition in DSC according to Schick and co-workers[40] employing such normalization on the measured ΔC_p. Similar results have been obtained in previous work for PDMS/silica and PDMS/titania nanocomposites, where the nanoparticles were generated by sol–gel method in the presence of crosslinked PDMS.[11,12] Following that work, we calculate this fraction of immobilized polymer from the relative reduction of $\Delta C_{p,n}$ (Table II) and get values of 0.69 and 0.72 for PS300/PDMS and ST/PDMS (preheating at 80°C), respectively.

The second main result (Table II) refers to the effects of nano-oxides on the crystallization behavior of PDMS. Next to the reduction of the crystallization temperature in the nanocomposites (from −78°C for neat PDMS to −99 and −88°C for PS300/PDMS and ST/PDMS, respectively), we observe (Table II) a reduction of the degree of crystallinity from 0.8 for neat PDMS to 0.2 and 0.67 for PS300/PDMS and ST/PDMS (preheated at 80°C), respectively, and the $X_{c,cryst}$ values are slightly higher than values of $X_{c,melt}$. Thus, by comparing each other the two types of nanocomposites (Table II) we can conclude that silica/titania is less effective than silica in suppressing X_c and reducing T_c due to a smaller fraction of the interfacial PDMS in ST/PDMS. Notice that employing similar study of core/shell system with fumed silica ($S = 290$ m^2/g) / PDMS-1000, in which silica particles were also modified by 4 wt % of iron oxide (Fe_2O_3), similar effects were revealed on both the suppression of X_c and ΔC_p.[41]

TSDC Measurements

The TSDC thermograms [Figure 6] are compared for neat PDMS and composites with PS300/PDMS and ST/PDMS. The depolarization currents are normalized by dividing by the applied electric field (giving units A m^{-1} V^{-1}).[37] These fields were varied for different samples due to the geometrical characteristics of the capacitor (i.e. thickness and diameter). After normalization, TSDC results for different samples can be compared to each other not only with respect to the temperature position of peaks (time scale of the corresponding relaxation) but also with respect to the magnitude of peaks (dielectric strength of the corresponding relaxation, $\Delta\varepsilon$).[38]

In the temperature range from −140 to −80°C, complex spectra consisting of three peaks are well discerned [Figure 6(b)]. Bearing in mind the similar range of equivalent frequencies of TSDC and DRS measurements,[37] we suggest at this stage that the three peaks (relaxations), called α, α_c and α' in the order of increasing temperature, are related to cooperative PDMS chain motions in the glass transition region.

For pure PDMS-1000, a single peak is observed at −129°C, which corresponds to the primary α relaxation associated with the glass transition of the amorphous phase of PDMS [Figure 6(b), curve 1]. The temperature T_α of the peak maximum, which is, in general, a good measure of T_g,[37] is in good agreement with the DSC data (Table II). In addition, a shoulder appears on the high-temperature side of the main peak extending up to approximately 15°C higher, its intensity being rather

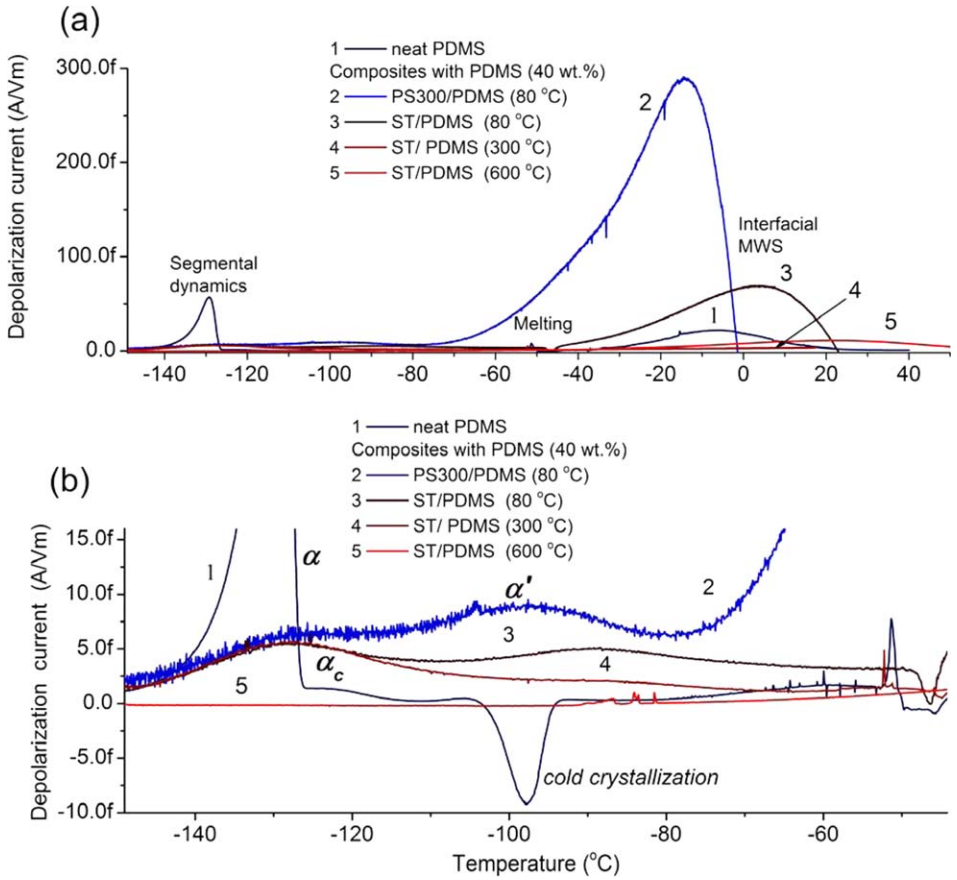

Figure 6. Comparative TSDC thermograms for initial PDMS, PS300/PDMS and ST/PDMS samples (a) overall behavior and (b) in the region of glass transition. [Color figure can be viewed in the online issue, which is available at wileyonlinelibrary.com.]

weak. The shoulder in the TSDC thermograms of initial PDMS is assigned to the α_c relaxation that corresponds to the mobility (dynamics) of amorphous polymer which is constrained-confined within the polymer crystals.[11,12] The main relaxation at −129°C in the nanocomposites is assigned to the α relaxation of the PDMS chains that are sufficiently far from the filler surface as to exhibit quasi-bulk behavior. For PS300/PDMS [Figure 6(b), curve 2] and ST/PDMS [Figure 6(b), curves 3 and 4] nanocomposites, the α relaxation is observed at approximately the same temperature but with a lower intensity.

The third peak in the TSDC thermograms of the composites is assigned to the α' relaxation of PDMS chains in an interfacial layer close to a surface of silica (or silica/titania) particles, where the chain mobility is constrained due to PDMS interactions with several adjacent nanoparticles (hydrogen bonding between the O atoms in the polymer backbone and the hydroxyls on the nanoparticle surface and van-der-Waals interactions between macromolecules and oxide surface).[42] Opposite to DSC, in which the interfacial polymer does not contribute in glass transition (decreasing ΔC_p),[12,40–42] in TSDC, the interfacial polymer mobility is recorded as an extra relaxation mechanism with slower dynamics (at higher temperatures) as compared to bulk mobility (i.e., α and α_c relaxations).[12,41–43]

Results in Figure 6(b) suggest that the α' relaxation is stronger in the case of the PS300/PDMS sample as compared to others. This would suggest a higher amount of polymer in the filler-polymer interfacial layer, with reduced mobility, for this sample. In the case of ST/PDMS sample, the α' relaxation, although being weaker, is shifted toward higher temperatures (up to −88°C), suggesting higher suppression of interfacial mobility than that of PDMS bound to unmodified silica.[12] Both results with respect to temperature position and relative magnitude of the α' peak will be quantified and discussed in the next section in relation to DRS results.

It is interesting to note that as the calcination temperature of the samples increases (above 300°C) the overall dielectric response of the samples is suppressed in the glass transition region (i.e., −140 to −80°C). In the extreme case of ST/PDMS, which was preheated at 600°C [Figure 6(b), curve 5], no relaxations are recorded in that region, suggesting practically total decomposition of the polymer. This result confirms suggestion that a portion of the products of PDMS depolymerization can modify the ST surface since the C—H stretching vibrations are observed in the FTIR spectra after similar treatment of the composites [Figure 1(b,c)].

Events recorded in the temperature range between −100 and −80°C seem to be related to cold crystallization.[36] The reason for recording cold crystallization by TSDC is the low heating rate used in this technique (3°C/min against 10°C/min in DSC measurements), by which it is given more time, comparing to

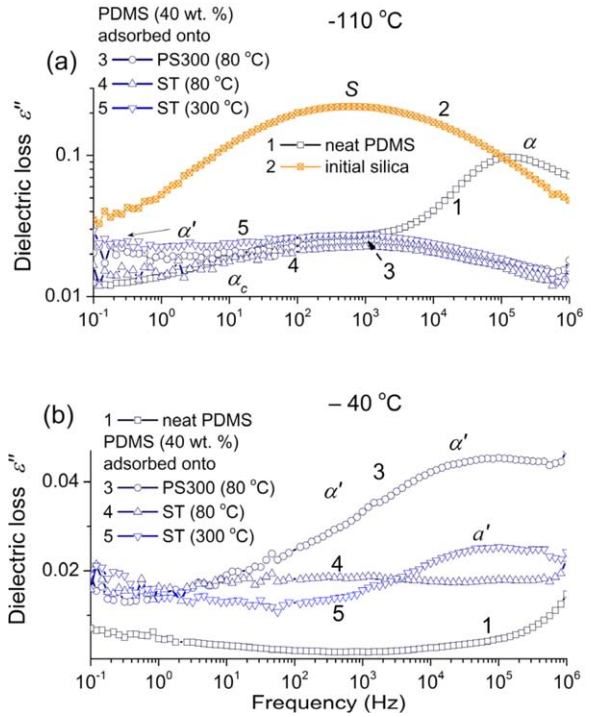

Figure 7. Comparative isothermal DRS plots of the imaginary part of dielectric permittivity ε'' versus frequency for initial PDMS (1), initial silica (2), PS300/PDMS (80°C) (3), ST/PDMS (80°C) (4), ST/PDMS (300°C) (5) at the temperatures of −110°C (a) and −40°C (b). [Color figure can be viewed in the online issue, which is available at wileyonlinelibrary.com.]

DSC, for the further development of crystallization, while passing through the T_c region [Figure 6].

At temperatures higher than those of the α and α′ TSDC peaks, a sharp low-intensity peak is observed in the thermograms [Figure 6] for all the samples between −60 and −40°C and a broad peak between −60 and 40°C. The sharp low-intensity peak is located in the temperature region of melting, which in combination with its small width makes it reasonable to associate it with melting in the crystalline regions of PDMS. The strong peak [Figure 6(a)], which increases in magnitude for PS300/PDMS sample [Figure 6(a), curve 2] and shifts toward higher temperatures in the presence of silica/titania nanoparticles [Figure 6(a), curves 3–5] in comparison with neat PDMS, is assigned to interfacial Maxwell–Wagner–Sillars polarization/relaxation. This mechanism corresponds to trapping of charge carriers (ions) at the interfaces between regions of different conductivity during the polarization step and their release during the depolarization step.[44]

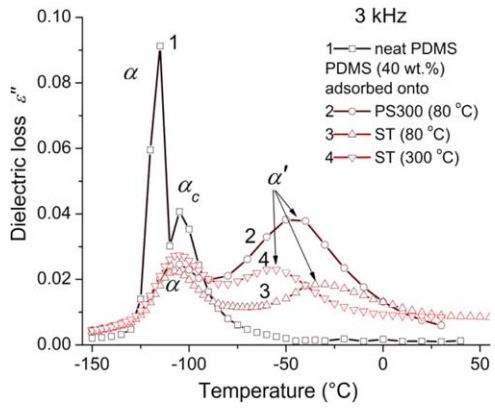

Figure 8. Comparative isochronal DRS plots of the imaginary part of dielectric permittivity ε'' versus temperature at 3 kHz for initial PDMS (1), PS300/PDMS (80°C) (2), ST/PDMS (80°C) (3), ST/PDMS (300°C) (4). [Color figure can be viewed in the online issue, which is available at wileyonlinelibrary.com.]

DRS

DRS was used to investigate the molecular dynamics in the bulk and interfacial layers of PDMS by following the temperature dependence of the corresponding dielectric relaxation. Note that DRS and TSDC are complementary to each other in the sense that the frequency range of TSDC corresponds to 10^{-2}−10^{-4} Hz,[45] which is a frequency region where DRS measurements are very difficult to be performed.[37]

DRS results will be comparatively presented here in the form of frequency (Figure 7, isothermal plots) or temperature dependence of the imaginary part of dielectric permittivity (dielectric loss) ε'' (Figure 8, isochronal plots). Data have been recorded isothermally and have been re-plotted in Figure 8 to facilitate comparison with the TSDC thermograms (Figure 6). A higher frequency of 3 kHz has been selected for the plots to suppress effects of conductivity.[38] The results agree well with those of TSDC, the slight shift toward higher temperatures in Figure 8, as compared to Figure 6, arising from the higher frequency of presentation.[42] Finally, the DRS results are analyzed by fitting model functions to the experimental data,[38] to evaluate the time scale (temperature dependence of the frequency maxima), the dielectric strength and the shape parameters of the recorded relaxations. To that aim we employed Havriliak–Negami (HN) equation[38]:

$$\varepsilon^*(f) = \frac{\Delta\varepsilon}{(1+(if/f_0)^{\alpha_{HN}})^{\beta_{HN}}}, \quad (4)$$

one term for each of three relaxations α, α_c, and α′, was fitted to the experimental data at each temperature and the fitting parameters (α_{HN}, β_{HN}) were determined. In this equation $\Delta\varepsilon$ is the dielectric strength, f_0 is a characteristic frequency related to the frequency of maximum loss (ε'') and α_{HN} and β_{HN} are the parameters of the relaxation shape. By plotting the frequency of maximum of ε'' against reciprocal temperature for the three segmental relaxations, the Arrhenius plot (activation diagram) was constructed (Figure 9). In Figure 10, we present the temperature dependence of $\Delta\varepsilon$ for selected samples.

We focus here on the segmental dynamics, that is, on the dielectric relaxations α, α_c, and α′ (Figure 7) corresponding to the TSDC response in the temperature range from −140 to −80°C (Figure 6). Isothermal plots (Figure 7) are shown at two temperatures, −110 and −40°C, properly selected for following three segmental relaxations α, α_c, and α′. The origin of these relaxations has been described in the previous section related to the TSDC results. The additional relaxation S [Figure 7(a), curve 2] was proposed to be attributed to motions of the silanol

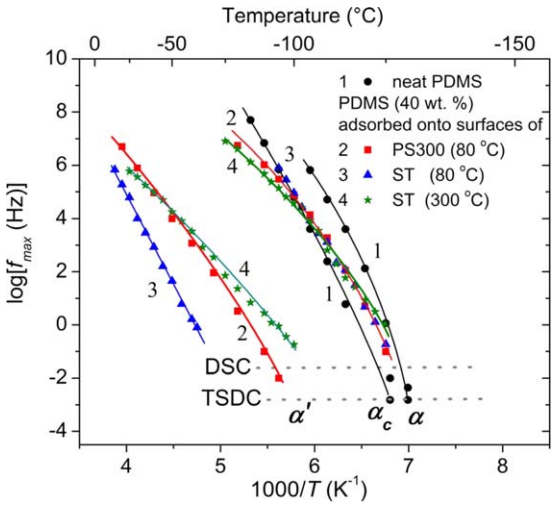

Figure 9. Arrhenius plots (activation diagram) of the segmental and interfacial dynamics for initial PDMS (1), PS300/PDMS (80°C) (2), ST/PDMS (80°C) (3), ST/PDMS (300°C) (4). Respective points were added from TSDC and DSC techniques. Dotted lines (···) were also added as guides for the eyes. [Color figure can be viewed in the online issue, which is available at wileyonlinelibrary.com.]

groups of silica (Si—OH) with attached water molecules.[29,41,42,46] The strength of the S relaxation should be related to the relative water content [(water molecules)/(number of Si—OH)] in the sample. The significant reduction of the magnitude of the S relaxation in the nanocomposites can be explained considering that most of the silanol groups must be engaged: (i) by the O atoms of water molecules in the case of initial oxide and (ii) by the O atoms in the PDMS backbone[12] or CH_3 groups of PDMS in nanocomposites.

The time scale of three relaxations can be discussed using the Arrhenius plot (frequency of maximum of ε'' vs. reciprocal temperature) shown for selected samples in Figure 9. The temperature dependence of its time scale of α and α_c are described by Vogel–Tammann–Fulcher–Hesse (VTFH) law[47] describing their

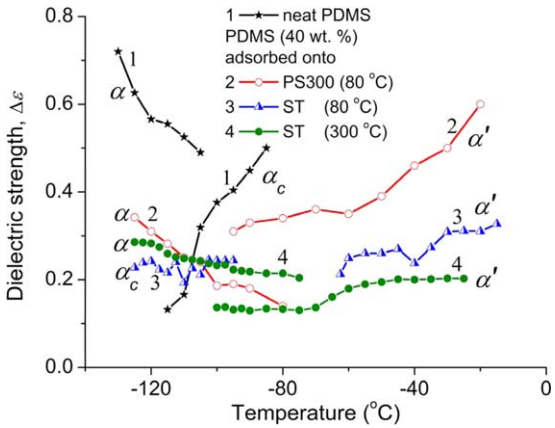

Figure 10. Dielectric strength, $\Delta\varepsilon$, versus temperature of the recorded dielectric relaxations for initial PDMS (1), PS300/PDMS (80°C) (2), ST/PDMS (80°C) (3), ST/PDMS (300°C) (4). [Color figure can be viewed in the online issue, which is available at wileyonlinelibrary.com.]

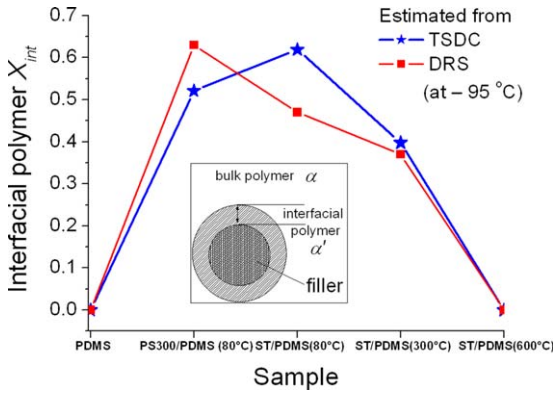

Figure 11. The fraction of PDMS with reduced mobility versus silica and silica/titania samples obtained from eq. (5). The inset shows the simplified model used to estimate the interfacial and bulk polymer phases. [Color figure can be viewed in the online issue, which is available at wileyonlinelibrary.com.]

cooperative character. After fitting VTFH equation to our experimental data we obtained values for the respective dielectric glass transition temperature values, $T_{g,\mathrm{diel}}$, for the equivalent frequency of DSC ($f = 1/\tau_{\mathrm{DSC}}$, where $\tau_{\mathrm{DSC}} \sim 100$ s).[12,48] The values are listed in Table II.

DSC and TSDC data are included into the plot (Figure 9) at the equivalent frequencies of 10 and 1.6 mHz.[42,49] The time scale of all relaxations for the various samples can be discussed using such plots. A main observation (Figure 9) is that the α and α_c relaxations have very similar frequency–temperature traces for neat PDMS. On the other hand, α' tends to be strongly separated from α and α_c, and its time scale is practically described by a straight line (Arrhenius behavior)[12] characterized by relatively lower activation energy (~0.52 and ~0.50 eV for silica and silica/titania, respectively), as compared to α and α_c. This change in the temperature dependence of the time scale from the Vogel–Tammann–Fulcher behavior for α and α_c, characteristic for cooperative processes, similar to the glass transition (more Arrhenius behavior for α') characteristic for local processes,[47] can be understood in terms of a thin interfacial layer with a thickness comparable to the cooperativity length of the glass transition.[42,47]

In Figure 10, the α' relaxation recorded is stronger for PS300/PDMS as compared to ST/PDMS, possibly reflecting the higher interaction polymer-particles in the first system. Conversely, in ST/PDMS the strength of α' was suppressed for the sample preheated at 80°C, comparing with the one calcined at 300°C, suggesting partial decomposition of the interfacial polymer layer of the first sample.

The results in $\Delta\varepsilon$ could be evaluated better employing a simple model of an interfacial layer with reduced mobility (giving rise to the α' relaxation),[48] depicted in the inset in Figure 11. We were able to estimate the reduced mobility polymer fraction, that is, the fraction of polymer in the interfacial layer, X_{int}, by the following equation:

$$X_{\mathrm{int}} = \frac{\Delta\varepsilon_{\alpha'}}{\Delta\varepsilon_{\alpha'} + \Delta\varepsilon_{\alpha}}, \qquad (5)$$

where $\Delta\varepsilon$ is the dielectric strength of each relaxation.[12,41] In the simple model (Figure 11) in eq. (5), α represents the whole

bulk behavior, that is, it includes also the α_c relaxation. It is good to note again, at this point that in DRS measurements X_{int} was estimated through the direct and additive contribution of the nanoparticles to the segmental dynamics (α' relaxation), whereas in DSC measurements we estimate the immobilization of the interfacial polymer more indirectly through the missing of the corresponding contribution to the heat capacity jump at the glass transition (reduction of the ΔC_p step). In addition to DRS, X_{int} is calculated from the TSDC data, by taking the surface area under the loss peak as a measure of the dielectric strength of the corresponding relaxation.[45,48]

Results for X_{int} are shown in Figure 11. As $\Delta\varepsilon$ determined by DRS is temperature dependent (Figure 10), a representative temperature of $-95°C$ was considered for the calculations shown in Figure 11. Results by the two techniques are in rather good agreement to each other, bearing in mind the last comment about temperature dependence of $\Delta\varepsilon$ and, thus, of X_{int} determined by DRS, the simplicity of the employed model, and experimental and calculation uncertainties. The maximum interfacial polymer fraction is 0.63 for the PS300/PDMS (calcination temperature 80°C), calculated by DRS, whereas for the ST/PDMS X_{int} decreases with increasing calcination temperature. It is interesting to compare results with those of a previous work on PDMS/silica nanocomposites, where silica was generated by sol–gel method in the presence of crosslinked PDMS.[42,48] Silica fraction was much lower there, compared to 60 wt % in the present work, and X_{int} were around 0.30 for a filler fraction of 25 wt %.

A final comment refers to comparison between DSC and dielectric results (DRS and TSDC) and apparent contradiction: immobilization of a fraction of polymer in the interfacial layer (no contribution to the glass transition) by DSC against reduced mobility in the interfacial layer (α' relaxation) by DRS and TSDC. Notice that the good agreement between values determined by DSC for the fraction of immobilized polymer in the interfacial layer and values determined by DRS and TSDC for the fraction of polymer with reduced mobility. Similar results were obtained in a previous work mentioned above on PDMS/silica nanocomposites, where silica was generated by sol–gel in the presence of crosslinked PDMS,[42,48] as well as in natural rubber/silica nanocomposites.[50] These results were rationalized by considering that in the interfacial layer configurational entropy is reduced due to restrictions imposed by the filler surface.[50] The changes in chain conformation in the nanocomposites may be also at the origin of the slight reduction of T_g in the nanocomposites, as compared to neat PDMS, reported in section "TSDC Measurements".

CONCLUSION

It was found that ST/PDMS composites are characterized by larger values of the contact angle of a water drop than PS300/PDMS. Analysis of the FTIR data demonstrated that for the PS300/PDMS pretreated at 400°C the band of the CH-stretching vibrations of CH_3 groups is absent in the FTIR spectra, while for the ST/PDMS, calcinations even to 650°C does not lead to a complete disappearance of this band. This difference can be explained by PDMS depolymerization at a ST surface at lower temperatures than that for PS300/PDMS that provides reactions of the depolymerization products with the oxide surface. The Si—O—Si(—)$(CH_3)_2$ groups can be crosslinked at the surface that increase their thermal stability. This leads to the mentioned observation of the C—H stretching vibrations for ST/PDMS samples preheated at $T > 500°C$ in contrast to PS300/PDMS. Additionally, the PDMS layer is thicker at the ST particle surface than that at PS300. Therefore, certain features of PDMS bound to ST can be close to bulk PDMS than that bound to PS300.

Molecular dynamics in a series of silica/PDMS and silica/titania/PDMS nanocomposites differently preheated were studied using DSC and dielectric techniques. The two dielectric techniques employed, DRS and TSDC, are complementary to each other, covering together a large frequency range, thus allowing the observation of the segmental dynamics of the polymer in a large range of time scales. Three discrete relaxations in the region of the glass transition were identified and studied, arising from the segmental mobility of the bulk (unaffected) polymer (α relaxation), the mobility of polymer chains restricted between condensed crystalline regions (α_c relaxation), and the segmental dynamics in the interfacial polymer layer (α' relaxation). Analysis of these relaxations in terms of time scale and dielectric strength reveals distinct differences between the two types of oxides, which may be understood in terms of different particle size, specific surface area, interfacial interaction strength, and different temperature behavior of the adsorbed PDMS layer. The results obtained by the three techniques employed agree with each other in the overall picture of reduction of molecular mobility in the nanocomposites. There exist, however, distinct differences between the results obtained by DSC, on the one hand, and by the two dielectric techniques (DRS, TSDC), on the other hand, which may be rationalized in terms of chain conformations in the interfacial layer and should be further followed in future work.

ACKNOWLEDGMENTS

The authors are grateful to the People Programme (Marie Curie Actions) of the European Union's Seventh Framework Programme FP7/2007–2013/ under REA grant agreement n° PIRSES-GA-2013–612484 for financial support. I.S. acknowledges support by the Visegrad Fund (Poland) (Contract number 51300077). This research has been co-financed by the European Union (European Social Fund – ESF) and Greek national funds through the Operational Program "Education and Lifelong Learning" of the National Strategic Reference Framework (NSRF) – Research Funding Program: Heracleitus II, Investing in knowledge society through the European Social Fund (P.K. and P.P.) and Research Funding Program: Aristeia (P.P.).

REFERENCES

1. Hu, J.; Zhou, Y.; He, M.; Yang, X. *Mater. Lett.* **2014**, *116*, 150.
2. Chapman, R.; Mulvaney, P. *Chem. Phys. Lett.* **2001**, *349*, 358.

3. Yoon, P. J.; Fornes, T. D.; Paul, D. R. *Polym. J.* **2002**, *43*, 6727.
4. Schmidt, G.; Malwitz, Matthew M. *Curr. Opin. Colloid Interface Sci.* **2003**, *8*, 103.
5. Schmidt, H.; Jonschker, G.; Goedicke, S.; Menning, M. *J. Sol-Gel Sci. Technol.* **2000**, *19*, 39.
6. Schmidt, D.; Shah, D.; Giannelis, E. M. *Curr. Opin. Solid State Mater. Sci.* **2002**, *6*, 205.
7. Levresse, P.; Feke, D. L.; Manas-Zloczower, I. *Polym. J.* **1998**, *39*, 3919.
8. Wen, J.; Mark, J. E. *J. Appl. Polym. Sci.* **1995**, *58*, 1135.
9. Carriere, D.; Moreau, M.; Barboux, P.; Boilot, J.-P. *Langmuir* **2004**, *20*, 3449.
10. Voronkov, M. G.; Meleshkevich, V. P.; Yuzhelevsky, Y. A. Siloxane Bond; Nauka: Novosibirsk, **1976**.
11. Klonos, P.; Panagopoulou, A.; Kyritsis, A.; Bokobza, L.; Pissis, P. *J. Non Cryst. Solids* **2011**, *357*, 610.
12. Klonos, P.; Panagopoulou, A.; Bokobza, L.; Kyritsis, A.; Peoglos, V.; Pissis, P. *Polymer* **2010**, *51*, 5490.
13. Rodriguez Hernandez, J. C.; Monleon Pradas, M.; Gomez Ribelles, J. L. *J. Non Cryst. Solids* **2008**, *354*, 1900.
14. Rittigstein, P.; Priestley, R. D.; Broadbelt, L. J.; Torkelson, J. M. *Nat. Mater.* **2007**, *6*, 278.
15. Torkelson, J. M.; Priestley, R. D.; Rittigstein, P.; Mundra, M. K.; Roth, C. B. *AIP Conf. Proc.* **2008**, 982, 192.
16. Machemer, R. *Invest. Ophthalmol. Vis. Sci.* **1988**, *29*, 1771.
17. Cibis, P. A.; Becker, B.; Okun, E.; Cowan, S. *Arch. Ophthalmol.* **1962**, *681*, 590.
18. Jonas, J. B.; Budde, W. M.; Knorre, H. L. J. *Am. J. Ophthalmol.* **1999**, *128*, 628.
19. Jensen, M. K.; Crandall, A. S.; Mamalis, N.; Olson, R. J. *Arch. Ophthalmol.* **1994**, *112*, 1037.
20. Olson, R. J.; Caldwell, K. D.; Crandall, A. S.; Jensen, M. K.; Huang, S.-C. *Am. J. Ophthalmol.* **1998**, *126*, 177.
21. Apple, D. J.; Federman, J. L.; Krolicki, T. J.; Sims, J. C.; Kent, D. G.; Hamburger, H. A.; Cox, M. S.; Hassan, T. S.; Compton, S. M.; Thomas, S. G. *Ophthalmology* **1996**, *103*, 1555.
22. Kusaka, A.; Kodama, T.; Ohashi, Y. *Am. J. Ophthalmol.* **1996**, *121*, 574.
23. Senn P.; Schmid, M. K.; Schipper, I.; Hendrickson, P. *Ophthalmic Surg. Laser.* **1997**, *28*, 776.
24. Larkin, G. B.; Flaxel, C. J.; Leaver, P. K. *Ophthalmology* **1998**, *105*, 2023.
25. Ludwig, D. B.; Trotter, J. T.; Gabrielson, J. P.; Carpenter, J. F.; Randolph, T. W. *Anal. Biochem.* **2011**, *410*, 191.
26. Morarescu, D.; West-Mays, J. A.; Sheardown, H. D. *Biomaterials* **2010**, *31*, 2399.
27. Apple, D. J.; Isaacs, R. T.; Kent, D. G.; Martinez, L. M.; Kim, S.; Thomas, S. G.; Basti, S.; Barker, D.; Peng, Q. *J. Cataract Refract. Surg.* **1997**, *23*, 536.
28. Kageyama, T.; Yaguchi, S. *J. Cataract Refract. Surg.* **2000**, *26*, 957.
29. Gun'ko, V. M.; Borysenko, M. V.; Pissis, P.; Spanoudaki, A.; Shinyashiki, N.; Sulim, I. Y.; Kulik, T. V.; Palyanytsya, B. B. *Appl. Surf. Sci.* **2007**, *253*, 7143.
30. Sulym, I. Y.; Borysenko, M. V.; Goncharuk, O. V.; Terpilowski, K.; Sternik, D.; Chibowski, E.; Gun'ko, V. M. *Appl. Surf. Sci.* **2011**, *258*, 270.
31. Gun'ko, V. M.; Turov, V. V.; Krupska, T. V.; Ruban, A. N.; Kazanets, A. I.; Leboda, R.; Skubiszewska-Zięba, J. *J. Colloid Interface Sci.* **2013**, *394*, 467.
32. Gun'ko, V. M.; Sulym, I. Y.; Borysenko, M. V.; Turov, V. V. *Colloids Surf. A* **2013**, *426*, 47.
33. Vansant, E. F.; Vander Voort, P.; Vrancken, K. C. Characterization and Modification of the Silica Surface; Elsevier: Amsterdam, **1995**.
34. Gun'ko, V. M.; Dyachenko, A. G.; Borysenko, M. V.; Skubiszewska-Zieba, J.; Leboda, R. *Adsorption* **2002**, *8*, 59.
35. Mack, G. L.; Angles D. A. The Determination of Contact Angles from Measurements of the Dimensions of Small Bubbles and Drops; Division of Chemistry: New York, **1935**.
36. Sorai, M. Comprehensive Handbook of Calorimetry and Thermal Analysis; Wiley: West Sussex, **2004**.
37. Brauenlich, P. Thermally Stimulated Relaxation in Solids; Springer: Berlin, **1979**.
38. Kremer, F.; Schoenhals, A. Broadband Dielectric Spectroscopy; Berlin: Springer, **2002**.
39. Aranguren, M. *Polymer* **1998**, *39*, 4897.
40. Sargsyan, A.; Tonoyan, A.; Davtyan, S.; Schick, C. *Eur. Polym. J.* **2007**, *43*, 3113.
41. Galaburda, M. V.; Klonos, P.; Gun'ko, V. M.; Bogatyrov, V. M.; Borysenko, M. V.; Pissis, P. *Appl. Surf. Sci.* **2014**, *305*, 67.
42. Fragiadakis, D.; Pissis, P. *J. Non Cryst. Solids* **2007**, *353*, 4344.
43. Holt, A. P.; Griffin, P. J.; Bocharova, V.; Agapov, A. L.; Imel, A. E.; Dadmun, M. D.; Sangoro, J. R.; Sokolov, A. P. *Macromolecules* **2014**, *47*, 1837.
44. Hedvig, P. Dielectric Spectroscopy of Polymers; Adam Hilger: Bristol, **1977**.
45. Vanderschueren, J.; Gasiot, J. *Top. Appl. Phys.* **1979**, *37*, 135.
46. Kirst, K. U.; Kremer, F.; Litvinov, V. M. *Macromolecules* **1993**, *26*, 975.
47. Donth, E. The Glass Transition: Relaxation Dynamics in Liquids and Disordered Materials. Springer Series in Materials Science; Springer: Berlin, **2001**.
48. Fragiadakis, D.; Pissis, P.; Bokobza, L. *Polymer* **2005**, *46*, 6001.
49. Vatalis, A. S.; Kanapitsas, A.; Delides, C. G.; Pissis, P. *Thermochim. Acta* **2001**, *372*, 33.
50. Fragiadakis, D.; Bokobza, L.; Pissis, P. *Polymer* **2011**, *52*, 3175.